A Numerical Cool-Down Analysis for Joule-Thomson Cryocoolers

N. Tzabar and A. Kaplansky

Cryogenics Group, Rafael
Haifa 31021, Israel

ABSTRACT

Joule-Thomson (JT) cryocoolers are commonly used for rapid cool-down of Infra-Red (IR) detectors. The cool-down time is governed both by the JT cryocooler performances and the Dewar structure, which is usually geometrically complicated. In order to calculate the exact temperature at every location of the Dewar as a function of time, a finite-element model of the complete Dewar-Detector-Cooler Assembly (DDCA) is developed. Since the isenthalpic expansion at the orifice can not be modeled with the finite-element code, the coolant state at the orifice outlet is provided with a predetermined table. The analysis calculates the heat transfer in the Dewar and the JT cryocooler, the coolant flow rate, and the pressure drop in the vessel that supplies the coolant to the JT cryocooler. A verification of the analysis is conducted against experimental results with a pressure vessel of 60 cc filled with argon at 69 MPa and 23°C. The model is further validated against other experimental results, without any change in its parameters, with pressure vessels of 60 cc and 150 cc at -25°C, 23°C, and 60°C. A good agreement is obtained between the analysis and the experimental results.

INTRODUCTION

Miniature JT cryocoolers for fast cool-down operate with pressurized fluids stored in pressure vessels which are discharged during operation. The cool-down time is defined as the time duration from the start of pressure vessel discharge until the device that has to be cooled reaches its operating temperature. The cool-down process duration may vary between a few seconds to a few minutes. This process includes extreme changes in the cooling power of the JT cryocooler.

Numerical studies of JT cryocoolers usually consider the device that has to be cooled as a lumped heat capacity [1-4], while in practice it usually has a complicated structure. Due to this complicated structure, the temperature reduction of the Dewar components is strongly governed by the ability of the Dewar structure to conduct the heat, and thus the cool-down time is limited. In a previous study we determined the limit at which further increase of the JT cryocooler flow rate did not improve the cool-down rate [5].

In the present study a finite-element analysis of a DDCA with a JT cryocooler is developed and implemented using the Ansys™ code. The model is axisymmetric; thus, the Dewar-Detector Assembly (DDA) is fully simulated and its heat transfer is calculated directly. On the other hand, the JT cryocooler has to be simulated in a more sophisticated manner in order to describe the

Cryocoolers 17, edited by S.D. Miller and R.G. Ross, Jr.

finned-tube heat exchanger, the expansion in the orifice, the jet emanating from the orifice, and the two-phase flow in the evaporator. In this study the model is described, the verification against experimental results is demonstrated, and further validation of the model is shown.

FINITE-ELEMENT MODEL DESCRIPTION

General

In the present study we developed an axisymmetric finite-element model of a DDCA in which the JT cryocooler is fed from a pressure vessel. A general view of a DDCA is shown in Figure 1. The JT cryocooler has a high pressure inlet fitting, a finned-tube heat-exchanger, an expansion orifice, and an evaporator. The Dewar contains of the IR detector, a cold-shield and two temperature sensors, T_A and T_B. A schematic view of the JT cryocooler with the pressure vessel is described in Figure 2. The high pressure coolant enters the JT cryocooler at the ambient temperature in point 1. The coolant flows through the high pressure side of the heat-exchanger to point 2, which is the inlet to the expansion orifice. The coolant leaves the orifice, point 3, where its pressure and temperatures are reduced and enters the evaporator, where most of the heat is removed from the Dewar. The coolant leaves the evaporator, point 4, and enters the low pressure side of the heat-exchanger. Finally, the coolant exits the JT cryocooler, point 5, at the ambient pressure.

The Dewar Detector Assembly (DDA) is modeled in a straight-forward manner while components that are not axisymmetric are modeled with their exact volume and their properties (specific heat capacity and heat conduction coefficient) are adjusted to maintain their actual values. On the other hand, the JT cryocooler is modeled indirectly, using a single fluid element to simulate all coolant states in the model. The radiation heat transfer is neglected in order to simplify the model and reduce the calculation time.

Expansion orifice

The coolant expands in the orifice in an isenthalpic process, points 2 to 3 in Figure 2, and both its pressure and temperature are reduced, while maintaining $h_3 = h_2$ (where h is the enthalpy). Since Ansys is not capable of determining such a process, a table has been prepared to provide the temperature of the coolant at point 3, T_3, as a function of the temperature and pressure at point 2, T_2 and p_2, respectively. The pressure at point 3, p_3, is assumed to be equal to the pressure at point 5, p_5, which equals the ambient pressure. Another pre-calculated table provides the liquid fraction, F_L, of the coolant in the orifice outlet, point 3, as a function of the temperature and pressure of the coolant in the orifice inlet, point 2.

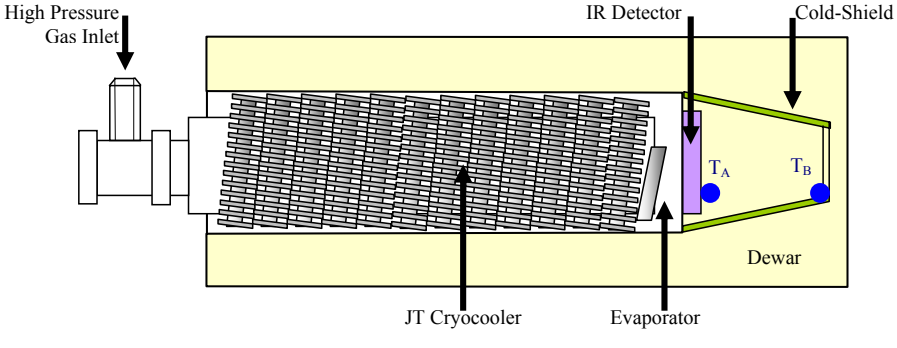

Figure 1. A schematic view of a DDCA.

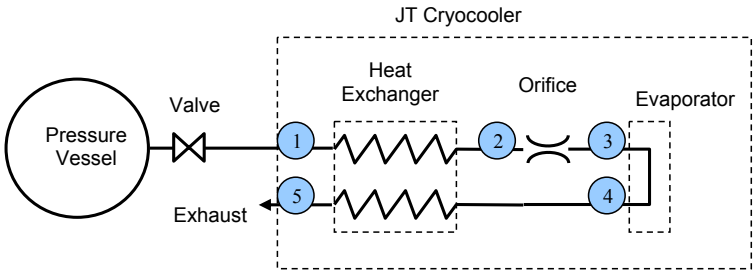

Figure 2. A schematic view of the JT cryocooler and the pressure vessel.

The flow rate of the coolant is determined by the orifice cross section area. Practically, we define the orifice size with a Free Flow Rate (FFR) parameter, which is the coolant flow through the orifice at 6.9 MPa and room temperature. The flow rate of the JT cryocooler is usually determined as follows:

$$\dot{m} = A \cdot C \cdot \sqrt{\frac{\kappa}{\left(\frac{\kappa+1}{2}\right)^{\kappa+1/\kappa-1}}} \cdot \frac{p}{\sqrt{R \cdot T}} \tag{1}$$

where $\dot{m}$ is the flow rate, A is the cross section area of the orifice, $\kappa=c_p/c_v$, R is the universal gas constant, and T and p are the temperature and pressure in the orifice inlet, respectively. C is a coefficient that depends on the temperature and pressure in the orifice inlet and is pre-detemined and provided to the model in a table. The equation in use for determining the flow rate in the present analysis is:

$$\dot{m} = FFR \cdot C \cdot \frac{p}{6.9}\sqrt{\frac{296}{T}} \tag{2}$$

where p is in MPa and T is in K.

Evaporator

The evaporator, between points 3 and 4 in Figure 2, is where the coolant reaches its two-phase state and most of the heat is removed from the DDA. The evaporator model is shown schematically in Figure 3. The coolant flows from point 3 to point 4 (same points as in Figure 2) through the pipe elements represented by the thick line. Each node along this pipe is connected with highly heat conductive elements (the thin dashed lines) to the evaporator walls. A convective heat transfer may be accounted in the selected elements by calculating the Nusselt number as follows:

$$Nu = N_1 + N_2 \cdot Re^{N_3} \cdot Pr^{N_4} \tag{3}$$

where Re is the Reynolds number, Pr is the Prandtl number, and N_1 to N_4 are dimensionless parameters.

The coolant enters the evaporator at a very high speed and meets the Dewar as an impinging jet. The convective heat transfer coefficients for impinging jets usually depend on the B/H ratio, where B is the orifice diameter and H is the distance between the orifice and the heat transfer surface [6,7], shown in Figure 3 as the distance between the cryocooler and the Dewar. Chen et al. [8] propose correlations for different B/H ratios. In the present study we fitted the following correlation for the evaporator:

$$Nu_e = 1.29 \cdot Re^{0.42} \cdot Pr^{0.65} \tag{4}$$

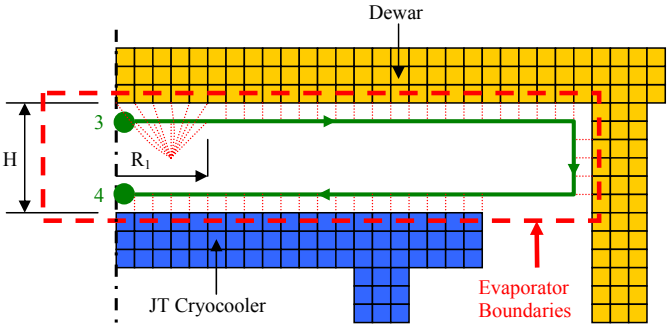

Figure 3. A schematic view of the evaporator model.

The impingement area is shown in Figure 3 with R_1. In this section the pipe nodes are connected to the Dewar surface nodes by high heat conductive elements that are all connected together, in order to equally distribute the heat flux.

Since the numerical code does not solve two-phase flow, we simulated the two-phase state by defining the coolant as a saturated liquid at its boiling temperature, T_b, and as a super heated vapor at T_b + 0.5 K. In this temperature range the density, the thermal conductivity, and the viscosity are calculated as follows:

$$\varphi = \varphi_L \cdot F_L + (1 - F_L) \cdot \varphi_V \tag{5}$$

where φ_L and φ_V are the properties at saturated liquid and super heated vapor states, respectively. The specific heat capacity of the coolant in this temperature range is determined according to the following equation:

$$c_p = \left(\frac{2 \cdot h_{fg}}{\Delta T} + c_{p,v} \right) \cdot F_L + c_{p,v} \cdot (1 - F_L) \tag{6}$$

where h_{fg} is the heat of vaporization, $c_{p,v}$ is the specific heat capacity of the coolant in the super heated vapor state, and ΔT is the defined temperature range for the two-phase state.

Heat Exchanger

The heat exchanger in use is a Hampson type that consists of a finned-tube for the high pressure stream, while the low pressure stream flows upon the external surface of the finned-tube. A section of the heat exchanger with the flow directions is shown in Figure 4. This type of heat exchanger configuration has been widely investigated [2,9,10], but can not be directly simulated in an axisymmetric model. Thus, it is simulated in the present study as demonstrated in Figure 5. The mass of the finned-tube with its heat capacity and heat conductance is simulated with two cylinders; the first one simulates the fins and is attached to the cryocooler mandrel, and the second one is attached to the fins cylinder and simulates the tube. Their length is adjusted to fit the length of the cryocooler mandrel. The low pressure stream is simulated by N thin tubes, where N is the number of gaps between fins in a single lap of the heat-exchanger. Each tube stands for a single gap between two fins, the flow through it is $\dot{m}/N$, and its diameter is determined such that it maintains the correct pressure drop between points 4 and 5 (see Figure 2). The length of each tube equals the length of the cryocooler mandrel; therefore, it has the same number and size of elements that are connected to the tube and fins cylinders via thermal conductor elements. The high pressure stream, shown in Figure 5 by the thick line, is a single tube with its original length which is much longer than the cryocooler mandrel, but with the same number of elements of the low pressure tubes. The thermal conduction elements between the high pressure tube and the tube and fins cylinders are also shown in Figure 5. There are several suggested equations for

calculating the convective heat transfer coefficient in finned-tubes heat exchangers. Gupta et al. (2009) have reviewed some equations from the literature and finally suggested the following [10]:

$$Nu_h = 0.023 \cdot Re^{0.8} \cdot Pr^{1/3} \tag{7}$$

$$Nu_c = 0.19 \cdot Re^{0.703} \cdot Pr^{1/3} \tag{8}$$

where Nu_h and Nu_c are the Nusselt number for the hot and cold streams, respectively, Hong et al. (2009) have suggested the following equations for the two streams [3]:

$$Nu_h = 0.023 \cdot Re^{0.8} \cdot Pr^{1/3} \cdot \left(1 + 3.5 \frac{d_{tube}}{d_r}\right) \tag{9}$$

$$Nu_c = 0.26 \cdot Re^{0.6} \cdot Pr^{1/3} \tag{10}$$

where d_{tube} is the inner diameter of the the high pressure tube, and d_r is the root diameter (the center of the helical tube diameter). Since the present study is an axisymmetric simulation of the original case, we used a general formula for both streams:

$$Nu = 1.63 + 0.08 \cdot Re^{0.7} \cdot Pr^{0.35} \tag{11}$$

During the model verification it was evident that the hydraulic diameter of the low pressure stream has to be multiplied by 3 in order to simulate the actual thermal performances and the pressure drop.

The coolant enters the high pressure tube at point 1 at the pressure of the vessel and the ambient temperature. It is assumed that the coolant reaches the ambient temperature due to the heat transfer along the connecting tube between the pressure vessel and the cryocooler. The coolant entering the low pressure tubes at point 4 is at vapor phase and its temperature equals the coolant temperature leaving the evaporator.

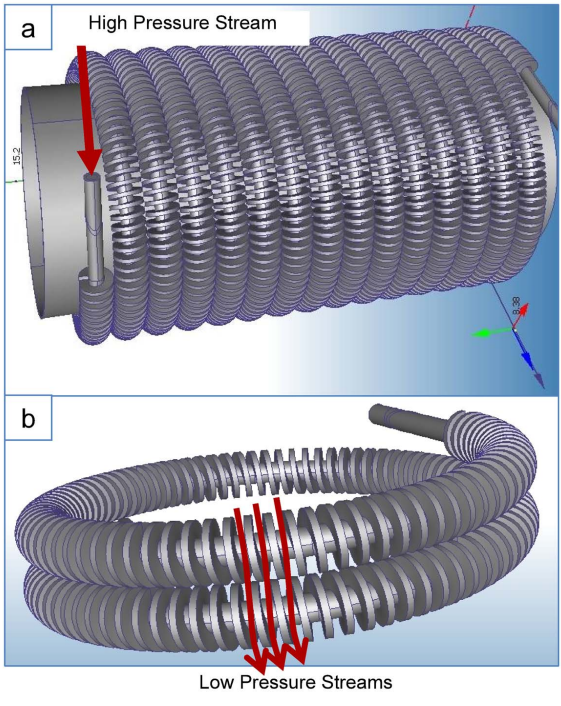

Figure 4. A heat exchanger with flow directions.

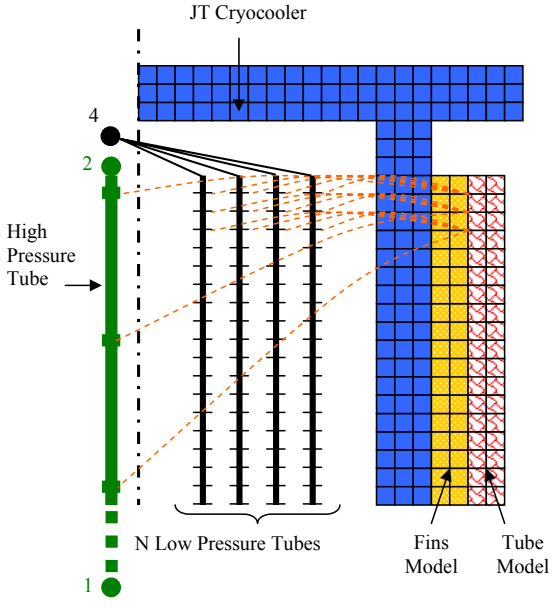

Figure 5. A schematic view of the heat-exchanger model.

Pressure Vessel

The volume of the pressure vessel, V, and the initial pressure, p_0, are known; thus, the initial coolant mass in the vessel, m_0, is determined. The calculations are made in time intervals of θ; therefore, the new coolant mass in the vessel is determined as follows:

$$m_{i+1} = m_i - \dot{m} \cdot \theta \tag{12}$$

where i and i+1 are time step indices. For each time step the density, ρ, is determined as follows:

$$\rho_i = \frac{m_i}{V} \tag{13}$$

The discharge process is assumed to be polytropic:

$$p \cdot v^n = \text{const.} \tag{14}$$

where n = 1 for an isothermal process and n = κ for an adiabatic process. In practice, n is between these values and the temperature of the coolant in vessel in step i+1 is found by calculating its entropy:

$$s_{i+1} = s(T_i, \rho_i) + \frac{\kappa - n}{\kappa - 1}\left[s(T_i, \rho_{i+1}) - s(T_i, \rho_i)\right] \tag{15}$$

The temperature is calculated as follows:

$$T_{i+1} = T_i - \left[T(s_i, \rho_i) - T(s_{i+1}, \rho_{i+1})\right] \tag{16}$$

The temperature is used to calculate the new pressure in the vessel.

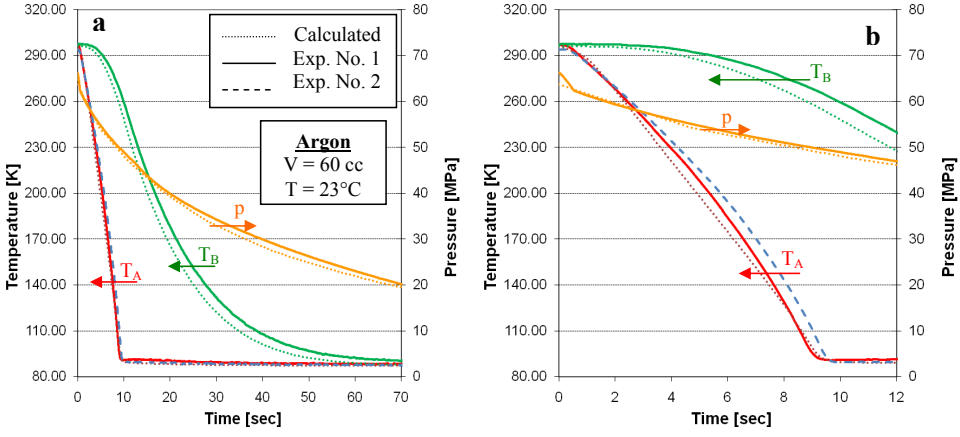

Figure 6. Verification of the analysis results, dotted lines, with two experimental results; Exp. 1 in solid lines and Exp. 2 in dashed line. Pressure vessel of 60 cc filled with argon at 69 MPa and 23°C. (a) shows the complete cool-down process and (b) shows a detailed view of the first 12 seconds.

RESULTS AND DISCUSSION

Model verification

The verification of the model was conducted against experimental results of JT cryocooler with FFR = 1.95, a 60 cc pressure vessel filled with argon at 69 MPa, and ambient temperature of 23 °C. during the verification process the following parameters were determined:

- The parameters in Eq. (4)
- The correction of the initial pressure in the model due to the pressure drop in the experiment caused by void volume between the vessel and the JT cryocooler
- The hydraulic diameter of the low pressure tube in the heat exchanger
- The radius of the impinging jet, R_1, where all nodes are connected
- The polytropic parameter, n

Figure 6 shows the analysis results, in dotted lines, with two experimental results; Exp. 1 in solid lines and Exp.2 in dashed line. Exp. 1 includes the results of T_A, T_B, and the vessel pressure, while Exp.2 has the results for T_A only. The accuracy of the temperature measurements is ± 0.5° and the accuracy of the pressure measurement is ± 0.34 MPa. The results show good agreement between the calculated and measured pressures which indicates correct calculations of temperature at the orifice inlet and mass flow rate. The calculated changes in T_B precede the experimental results for about 2.5 sec which is associated to the absence of the radiation heat load in the numerical model. Figure 6(b) is a detailed view of the cool-down process which emphasizes the good agreement between the analysis and the experimental results.

Model validation

First validation of the analysis was performed by comparing its results with the same JT cryocooler and the same pressure vessel, 60 cc, at different ambient temperatures: -25 and 60°C. The filling pressure is 69 MPa at 23°C, while all other parameters stay constant. The results for ambient temperatures of -25 and 60°C are shown in Figures 7, and 8, respectively. The good agreement between the calculations and experimental results is fully kept at -25°C, while at 60°C a delay of 1.5 sec is obtained for the calculated T_A relative to the experimental results. This deviation is acceptable due to the large rang of ambient temperature discussed.

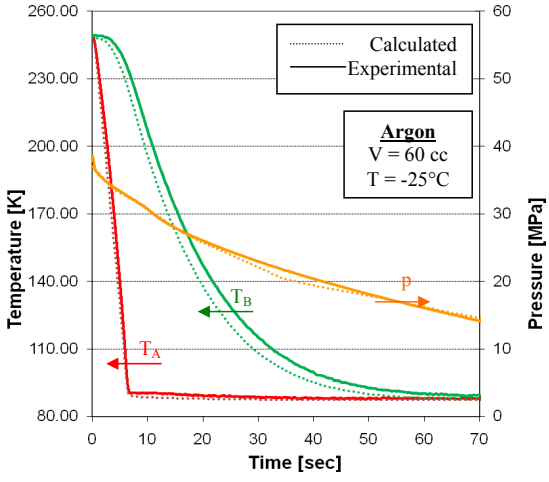

Figure 7. A comparison between the analysis results, dotted lines, and experimental results, solid lines at -25°C. Pressure vessel of 60 cc filled with argon at 69 MPa @ 23°C.

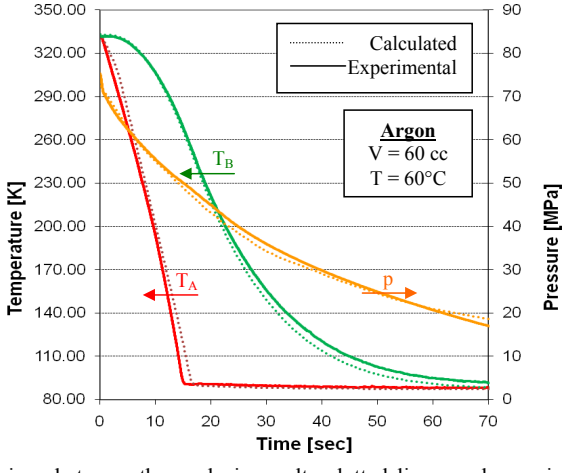

Figure 8. A comparison between the analysis results, dotted lines, and experimental results, solid lines at 60°C. Pressure vessel of 60 cc filled with argon at 69 MPa @ 23°C.

Figures 9, 10, and 11 show the results for the same JT cryocooler with another pressure vessel, 150 cc, at 23, -25, and 60°C, respectively. The results at 23°C show good agreement between the calculated and measured values of T_A in a similar manner as for the 60 cc pressure vessel. At ambient temperature of -25°C instability in the measured T_A is obtained; however, it is evident that the calculation prediction fits the experimental results well. Again, at ambient temperature of 60°C the calculated results lag behind the experimental results for about one second. For all cases, the calculated results of T_B precede the experimental results for a few seconds only, due to the absence of radiation heat transfer in the analysis. For both pressure vessels the calculated T_B precede the experimental T_B for about 4, 2.5, and 2.2 sec at -25, 23, and 60°C, respectively.

The results presented demonstrate the stability of the analysis over a wide range of operating conditions: ambient temperature range of 85° and pressure vessel volume from 60 to 150 cc. The maximum deviation of the calculated IR detector cool-down time relative to the experimental results is 1.5 sec at extreme ambient temperature of 60°C.

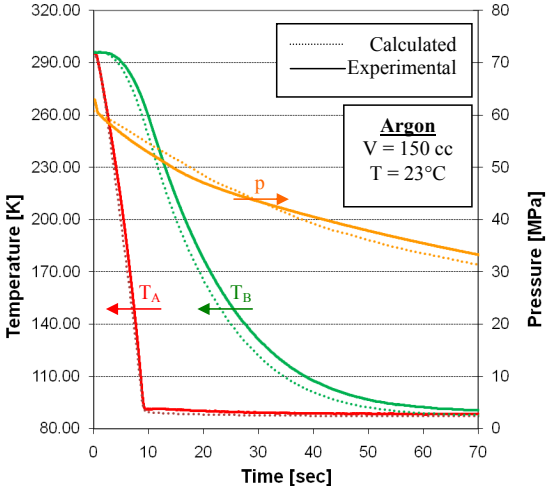

Figure 9. A comparison between the analysis results, dotted lines, and experimental results, solid lines at 23°C. Pressure vessel of 150 cc filled with argon at 69 MPa @ 23°C.

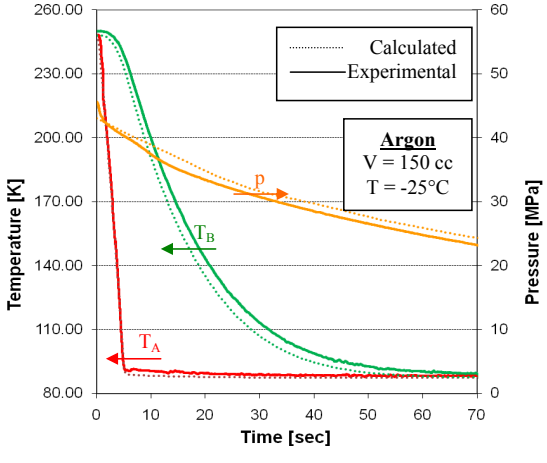

Figure 10. A comparison between the analysis results, dotted lines, and experimental results, solid lines at -25°C. Pressure vessel of 150 cc filled with argon at 69 MPa @ 23°C.

CONCLUSIONS

An approach for modeling a DDCA using a finite-element analysis is presented, and a detailed explanation about the JT cryocooler modeling procedure is provided. The model is suitable for calculating the heat transfer in the DDCA during the transient process of cool-down. The analysis is verified against experimental results at a single scenario and validated with other experimental results at different ambient temperatures and different pressure vessel volumes. A good agreement between the analysis results and the experimental results is obtained, even though the operating conditions are extremely different. This analysis enables the prediction of the cool-down performances of JT cryocooler during the development stages prior to prototype production. In addition, the analysis facilitates parameter and sensitivity studies.

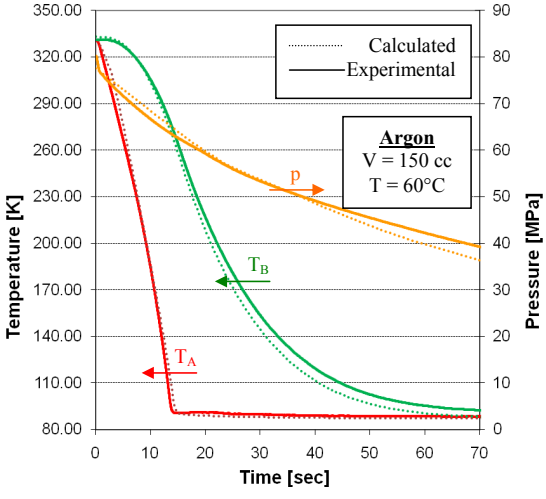

Figure 11. A comparison between the analysis results, dotted lines, and experimental results, solid lines at 60°C. Pressure vessel of 150 cc filled with argon at 69 MPa @ 23 °C.

REFERENCES

1. Chou F.C., Pai C.F., Chien S.B., and Chen J.S, "Preliminary experimental and numerical study of transient characteristics for a Joule-Thomson cryocooler," *Cryogenics*, vol. 35 (1995), pp. 311-316.
2. Chua H.T., Wang X., and Teo H.Y., "A numerical study of the Hampson-type miniature Joule-Thomson cryocooler," *International Journal of Heat and Mass Transfer*, vol.49 (2006), pp. 582-593.
3. Hong Y.J., Park S.J., and Choi Y.D., "A numerical study of the performance of a heat exchanger for a miniature Joule-Thomson refrigerator," *Cryocoolers 15*, ICC Press, Boulder, CO (2009), pp. 379-386.
4. Hong Y.J., Park S.J., and Choi Y.D., "A numerical study on the performance of the miniature Joule-Thomson refrigerator," *Advances in Cryogenic Engineering – CEC*, vol. 55 (2010), pp. 103-110.
5. Tzabar N., Lifshiz I., and Kaplansky A., "Fast cool-down J-T cryocooler to 88K," *Advances in Cryogenic Engineering – CEC*, vol. 53 (2008), pp. 1025-1032.
6. Michna G.J., Browne E.A., Peles Y., and Jensen M.K., "Single-phase microscale jet stagnation point heat transfer," *Journal of Heat Transfer*, vol. 131(2009), pp. 1-8.
7. Zhang P., Xu G.H., Fu X., and Li C.R., "Confined jet impingement of liquid nitrogen onto different heat transfer surfaces," *Cryogenics*, vol. 51 (2011), pp. 300-308.
8. Chen Y.C., Ma C.F., Qin M., and Li Y.X., "Forced convective heat transfer with impinging slot jets of meso-scale," *Int J of Heat and Mass Transfer*, vol. 49 (2006), pp. 406-410.
9. Gupta P.K., Kush P.K., and Tiwari A., "Design and optimization of coil-tube heat exchangers for cryogenic applications," *Cryogenics*, vol. 47 (2007), pp. 322-332.
10. Gupta P.K., Kush P.K., and Tiwari A., "Experimental research on heat transfer coefficients for cryogenic cross-counter-flow coiled finned-tube heat exchangers," *International Journal of Refrigeration*, vol. 32 (2009), pp. 960-972.